Noname manuscript No.
(will be inserted by the editor)

Polarization observables T and F in π^0 photoproduction off the proton with CLAS g9 experiment

H. Jiang · S. Strauch · (For the CLAS Collaboration)

Received: date / Accepted: date

Abstract Pion photoproduction in the $\gamma p \to \pi^0 p$ reaction has been measured in the FROST experiment at the Thomas Jefferson National Accelerator Facility. In this experiment, circularly polarized photons with energies up to 3.082 GeV impinged on a transversely polarized frozen-spin target. Final-state protons were detected in the CEBAF Large Acceptance Spectrometer. Preliminary results of the polarization observables T and F have been extracted. The data generally agree with predictions of present partial-wave analyses, but also show marked differences. The data will constrain further partial wave analyses and improve the extraction of proton resonance properties.

1 Introduction

The theory that describes the interaction of quarks is Quantum Chromodynamics (QCD), but how quarks are bound inside a nucleon is not yet well understood. Pion photoproduction experiments reveal important information about the nucleon excited states and the dynamics of the quarks within it and thus provide a useful tool to study QCD. There are several ways to probe the baryon excited states. In addition to the mass and width values provided by the elastic pion-nucleon scattering, the single-pion photoproduction process provides complementary data on the photo-couplings of the excited nucleon states and reaction amplitude. The extraction of the polarization observables T and F is possible from data with circularly polarized photons and transversally polarized target protons. The polarized cross section [1] with circularly polarized beam and transversely target can be simplified

This work is supported in parts by NSF PHY-1505615.

H. Jiang
University of South Carolina, Columbia, SC, USA

S. Strauch
University of South Carolina, Columbia, SC, USA

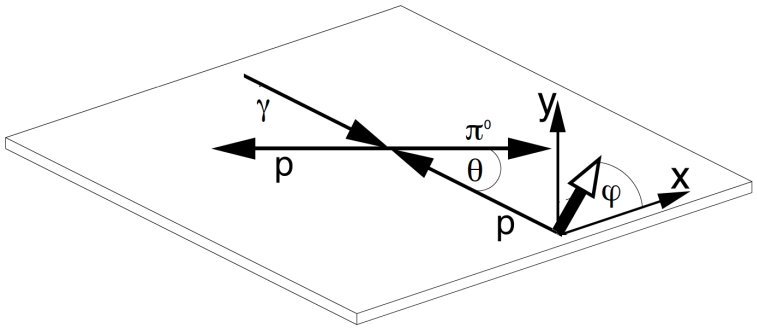

Fig. 1 Schematic of the $\gamma p \to \pi^0 p$ reaction in the center-of-mass frame with circularly polarized photon beam and transversally polarized target. The arrow with an open arrowhead indicates the target-polarization direction.

to

$$\frac{d\sigma}{d\Omega} = \frac{d\sigma_0}{d\Omega}\left(1 + P_T T \sin(\varphi) + P_T P_\odot F \cos(\varphi)\right), \tag{1}$$

where $P_\odot$ is the right-circular beam polarization, P_T is the degree of target polarization, and φ is the angle from the reaction plane to the target polarization direction. All other polarization observables, including the proton-recoil polarizations, are fully integrated out even with limited detector acceptance. The schematic of the reaction is shown in Fig. 1.

2 Experiment

This experiment, E03-105 "Pion Photoproduction from a Polarized Target", was conducted at the Thomas Jefferson National Accelerator Facility (Jefferson Lab). The data were taken as part of the g9 run group from March 18 to August 12, 2010, using the CEBAF large acceptance spectrometer (CLAS) [2] in Hall B at Jefferson Lab. The circularly polarized tagged photons with energies up to 3.082 GeV were produced in the radiator of the Hall-B Photon Tagger [3] by incident longitudinally polarized electrons with energies of 2.266 GeV and 3.082 GeV. The bremsstrahlung process produced the circularly polarized tagged photons from incident longitudinally polarized electrons. The polarization of the photon beam depends on the ratio between its energy E_γ and the electron energy E_0. Specifically, the degree of the circular polarization is expressed as [4]

$$P_\odot = P_e \frac{4x - x^2}{4 - 4x + 3x^2}, \tag{2}$$

where $x = E_\gamma / E_0$. Møller measurements [5] determined the electron-beam polarization. The average electron-beam polarization was $P_e = 0.873 \pm 0.005$. The photon-beam helicity was flipped pseudo-randomly at a rate of 240 Hz or 30 Hz. The collimated photon beam irradiated a frozen-spin butanol target (FROST) [6].

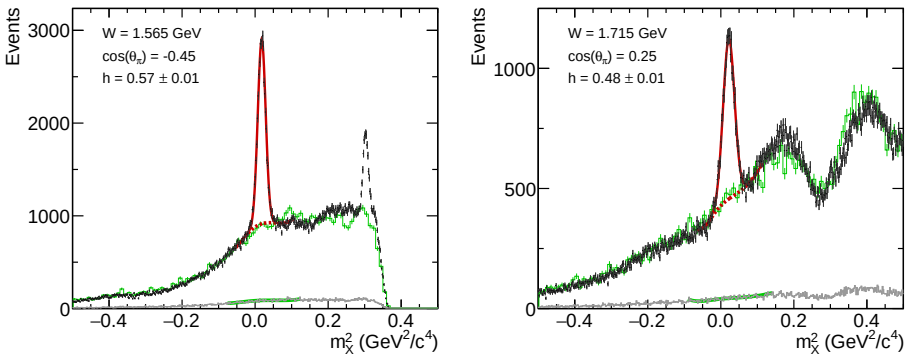

Fig. 2 Preliminary examples of missing-mass-squared distributions from butanol- (black histograms) and carbon-target data (gray histograms). The solid red and green curves are fits to the butanol and carbon data, respectively. The scaled carbon-data fits are shown as red dashed curves and the scaled carbon distributions as green histograms. Also indicated are the dilution factors h.

The nuclear spin of free protons in the target was transversally polarized. The degree of polarization ranged from 75% to 86%. The spin-lattice relaxation time during g9b was about 3400 h for positive polarization with beam on target and 4000 h without beam. The relaxation time for the negative spin state was about half that of the positive [6]. About once per week the target was repolarized and its polarization direction was reversed. Additional unpolarized carbon and polyethylene targets downstream of the butanol target helped clarify the bound-nucleon background and helped with the study of instrumental asymmetries.

3 Data Analysis

The final-state particles were detected by the CLAS. Events with one positively charged particle and zero negatively charged particles were considered in this analysis. The time-of-flight technique was used to identify the final-state protons. The channel identification was based on individual kinematic bins. The data were binned in W from 1.43 GeV to 2.51 GeV with a bin size of 0.03 GeV and in cosine of the center-of-mass angle, $\cos\theta_\pi^{cm}$, from -1 to 1 with a bin size of 0.1. The missing-mass-squared distributions (M_X^2) in the $\gamma p \to pX$ reaction from both butanol and carbon targets were accumulated for each bin. Figure 2 shows two examples of M_X^2 distributions for various energy and angular bins. The black histograms show data from the butanol target, while the gray histograms show data from the carbon target. The central peaks at $m_X^2 = m_{\pi^0}^2$ above a broad background correspond to events from the $\gamma p \to \pi^0 p$ reaction off free protons in the butanol target. A function was fit simultaneously to each distribution around the missing-π^0 peak to determine the bound-nucleon background in the missing-mass-squared distributions from the butanol target. The carbon-target distribution was described with a cubic spline; the butanol-target distribution was described by the same spline function multiplied by a scale factor for the bound-nucleon background and a Gaussian function for the free-proton signal events of the expected reaction channel. The scale factor is one of the fit parameters. In the end, the carbon-target

data had only a minor influence on the fit due to the small statistics of the carbon-target sample. Structures in the missing-mass-squared distribution above $m^2_{\pi^0}$ are due to free and quasifree photoproduction of multiple or higher-mass mesons. The slight mismatch between the butanol and the low-statistics carbon data is likely due to acceptance differences.

For each kinematic bin, the butanol-target events that satisfy the $\gamma p \to \pi^0 p$ kinematics were selected for further analysis. The selection was based on the condition

$$|M_X^2 - M_0^2| < 2\sigma_H, \tag{3}$$

where M_0^2 and σ_H were the peak position and peak width of the missing pion in the M_X^2 distribution. For those events, normalized polarized yields and dilution factors were calculated. The dilution factor h is the ratio between the number of free proton events and the total number of events.

The polarization observables T and F for a specific center-of-mass energy, W, and a specific cosine of the center-of-mass angle, $\cos\theta_\pi^{cm}$, were extracted from normalized Fourier moments of the measured events in the associated W and $\cos\theta_\pi^{cm}$ bin. From the expression of the polarized cross section, Eq. (1), the integrated normalized polarized yield of a specific bin can be expressed as

$$Y = \frac{1}{2\pi}\int_0^{2\pi} Y_{unpol} A(\varphi)(1 + P_T T \sin\varphi + P_T P_\odot F \cos\varphi) d\varphi, \tag{4}$$

where Y_{unpol} is proportional to the unpolarized cross section and $A(\varphi)$ is the average acceptance of the detector in the bin of interest. Experimentally, the normalized moments are obtained for each kinematic bin as

$$Y = \frac{\sum_i(1)}{N}, \quad Y_{\sin m\varphi} = \frac{\sum_i(\sin m\varphi_i)}{N}, \quad Y_{\cos m\varphi} = \frac{\sum_i(\cos m\varphi_i)}{N}, \tag{5}$$

where the sums are taken over the butanol-target events that satisfy the $\gamma p \to \pi^0 p$ kinematics. A relative normalization of the sums is given by the number of carbon-target events N from the respective setting, which is proportional to the luminosity. An overall absolute normalization cancels in the final expressions for the observables and can be safely neglected.

Since there are four combinations of two target-polarization directions and two photon-beam helicities, each of the normalized yields or moments can be categorized into four groups. In this analysis $+/-$ stands for the photon beam helicity and $\leftarrow/\rightarrow$ for the target polarization direction. By utilizing different combinations of target or beam polarizations, after determining the acceptance effect, the polarization observables T and F can be obtained from [7,8]:

$$T = \frac{1}{h}\frac{2(Y^{\rightarrow}_{\sin\varphi} - Y^{\leftarrow}_{\sin\varphi})}{P_T^{\leftarrow}(Y^{\rightarrow} - Y^{\rightarrow}_{\cos 2\varphi}) + P_T^{\rightarrow}(Y^{\leftarrow} - Y^{\leftarrow}_{\cos 2\varphi})} \tag{6}$$

and

$$F = \frac{1}{h}\frac{2(Y^{\rightarrow +}_{\cos\varphi} - Y^{\rightarrow -}_{\cos\varphi} - Y^{\leftarrow +}_{\cos\varphi} + Y^{\leftarrow -}_{\cos\varphi})}{P_\odot P_T^{\leftarrow}(Y^{\rightarrow} + Y^{\rightarrow}_{\cos 2\varphi}) + P_\odot P_T^{\rightarrow}(Y^{\leftarrow} + Y^{\leftarrow}_{\cos 2\varphi})}. \tag{7}$$

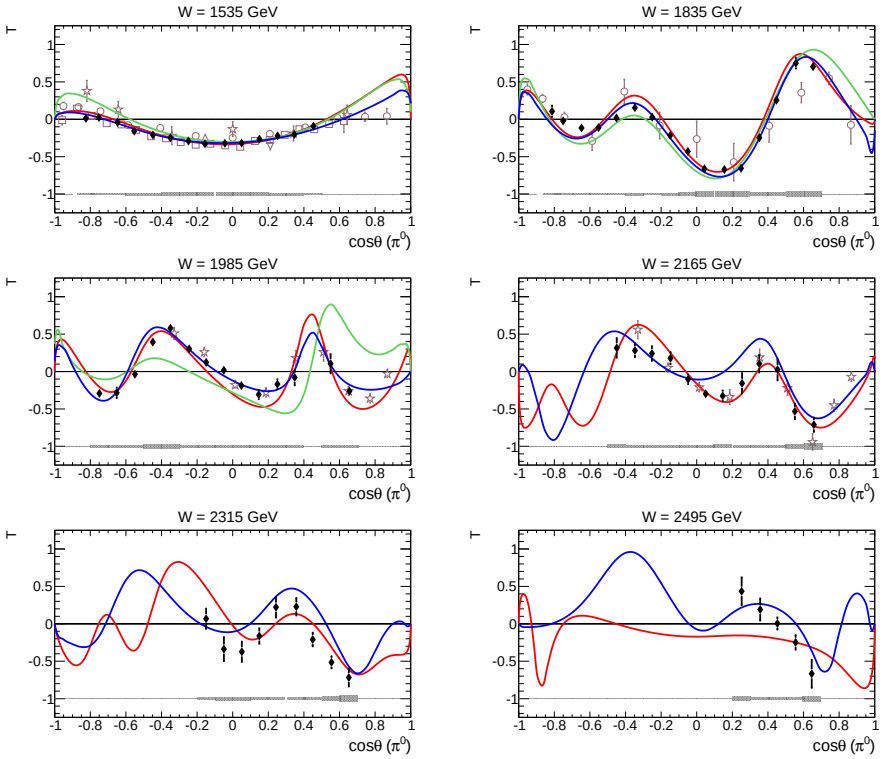

Fig. 3 Preliminary examples of polarization observable T. The preliminary results of this analysis are shown in black. The gray band indicates the size of the systematic uncertainties. The SAID (MA27) [9], BnGa (2014-02) [10], and MAID (2007) [11] model predictions are shown in red, blue, and green. Data from other experiments are also shown as circle (MAMI, Mainz [12]), square (CBELSA/TAPS, Bonn [13]), triangle (Institute for Nuclear Study, Tokyo [14,15]), and star (Daresbury Laboratory [16,17]).

4 Results

The preliminary results for the polarization observables T and F are shown in Figs. 3 and 4 for six out of 37 energy bins. The results of this analysis agree with previous measurements in the overlapping energy range. The major difference between the results of this analysis and the results from previous measurements is in the coverage of the energy range. In this analysis, the upper limit of W, 2525 MeV, is much higher than in previous measurements.

The preliminary results are compared with solutions from SAID (MA27) [9], BnGa (2014-02) [10], and MAID (2007) [11]. The present SAID, BnGa, and MAID model predictions generally agree with the data in the energy range that overlaps with previous measurements, but significant deviations are observed, mostly in the range of W above 2100 MeV. This meets the expectation of this analysis which is to constrain the partial-wave analyses and also improved the completeness of data from pion-photoproduction experiments. Partial-wave analyses of the present results have been started.

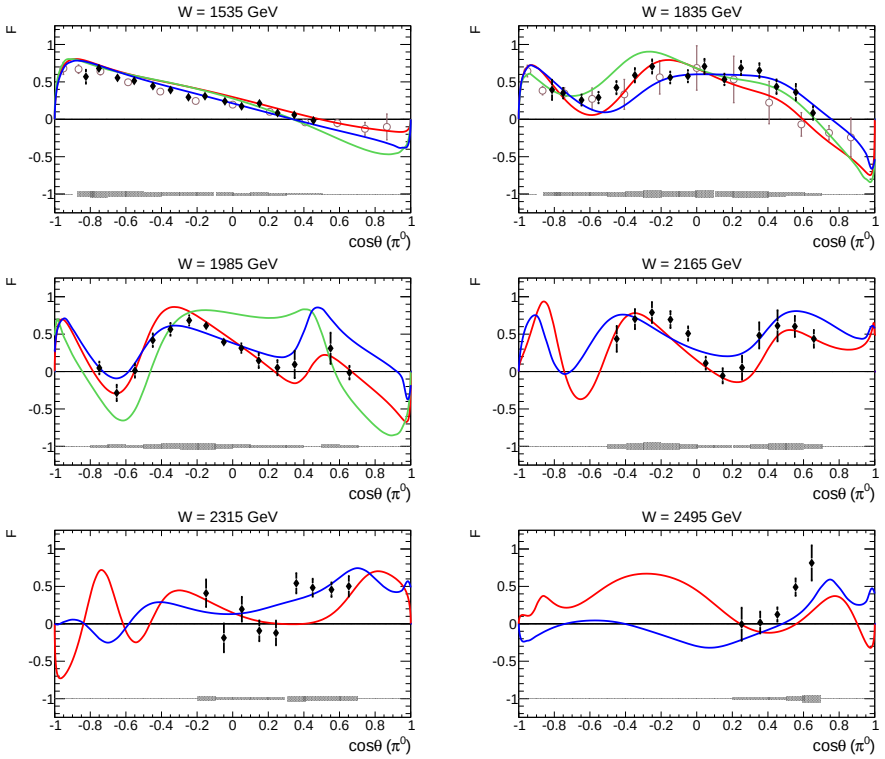

Fig. 4 Examples of polarization observable F. The preliminary results of this analysis are shown in black. The gray band indicates the size of the systematic uncertainties. The SAID (MA27) [9], BnGa (2014-02) [10], and MAID (2007) [11] model predictions are shown in red, blue, and green. Data from other experiments are also shown as circle (MAMI, Mainz [12]), square (CBELSA/TAPS, Bonn [13]), triangle (Institute for Nuclear Study, Tokyo [14,15]), and star (Daresbury Laboratory [16,17]).

The data of different observables, especially in the energy range that was not included in the previous measurement, become useful for the partial-wave analysis to fulfill the completeness in the determination of the pion-photoproduction reaction. The future data will constrain further partial-wave analyses and improve the extraction of proton resonance properties as polarization observables provide important constraints to reveal the dynamics and relevant degrees-of-freedom within hadrons.

References

1. I.S. Barker, A. Donnachie, J.K. Storrow, Nucl. Phys. **B95**, 347 (1975). DOI 10.1016/0550-3213(75)90049-8
2. B.A. Mecking, et al., Nucl. Instrum. Meth. **A503**, 513 (2003). DOI 10.1016/S0168-9002(03)01001-5
3. D. Sober, et al., Nucl. Instrum. Meth. A **440**, 263 (2000). DOI 10.1016/S0168-9002(99)00784-6
4. H. Olsen, L.C. Maximon, Phys. Rev. **114**, 887 (1959). DOI 10.1103/PhysRev.114.887

5. Circular Beam Polarization (2017). `https://clasweb.jlab.org/rungroups/g9/wiki/index.php/Circular_Beam_Polarization`
6. C. Keith, J. Brock, C. Carlin, S. Comer, D. Kashy, J. McAndrew, D. Meekins, E. Pasyuk, J. Pierce, M. Seely, Nucl. Instrum. Meth. A **684**(0), 27 (2012). DOI http://dx.doi.org/10.1016/j.nima.2012.04.067.
7. D. Besset, et al., Nucl. Instrum. Meth. A **166**(3), 515 (1979).
8. M. Dugger, et al., CLAS-Note 2008-05 (2008).
9. P.T. Mattione, et al., Phys. Rev. **C96**(3), 035204 (2017). DOI 10.1103/PhysRevC.96.035204
10. A.V. Anisovich, A. Sarantsev, O. Bartholomy, E. Klempt, V.A. Nikonov, U. Thoma, Eur. Phys. J. **A25**, 427 (2005). DOI 10.1140/epja/i2005-10120-5
11. D. Drechsel, S.S. Kamalov, L. Tiator, Eur. Phys. J. **A34**, 69 (2007)
12. J.R.M. Annand, et al., Phys. Rev. C **93**, 055209 (2016). DOI 10.1103/PhysRevC.93.055209
13. J. Hartmann, et al., Phys. Rev. Lett. **113**, 062001 (2014)
14. P. Feller, et al., Nucl. Phys. B **110**, 397 (1976)
15. M. Fukushima, et al., Nucl. Phys. B **136**, 189 (1978)
16. P. Booth, et al., Nucl. Phys. B **121**, 45 (1977)
17. P. Bussey, et al., Nucl. Phys. B **154**, 492 (1979)